

Infrared optical properties of Pr_2CuO_4

C. C. Homes*

Department of Physics, Brookhaven National Laboratory, Upton, NY 11973

Q. Li

Department of Materials Science, Brookhaven National Laboratory, Upton, NY 11973

P. Fournier[†] and R. L. Greene

*Center for Superconductivity Research, Department of Physics and Astronomy,
University of Maryland, College Park, MD 20742*

(Dated: November 1, 2018)

The *ab*-plane reflectance of a Pr_2CuO_4 single crystal has been measured over a wide frequency range at a variety of temperatures, and the optical properties determined from a Kramers-Kronig analysis. Above ≈ 250 K, the low frequency conductivity increases quickly with temperature; $\rho_{dc} \approx 1/\sigma_1(\omega \rightarrow 0)$ follows the form $\rho_{dc} \propto \exp(E_a/k_B T)$, where $E_a \approx 0.17$ eV is much less than the inferred optical gap of ≈ 1.2 eV. Transport measurements show that at low temperature the resistivity deviates from activated behavior and follows the form $\rho_{dc} \propto \exp[(T_0/T)^{1/4}]$, indicating that the *dc* transport in this material is due to variable-range hopping between localized states in the gap. The four infrared-active E_u modes dominate the infrared optical properties. Below ≈ 200 K, a striking new feature appears near the low-frequency E_u mode, and there is additional new fine structure at high frequency. A normal coordinate analysis has been performed and the detailed nature of the zone-center vibrations determined. Only the low-frequency E_u mode has a significant Pr-Cu interaction. Several possible mechanisms related to the antiferromagnetism in this material are proposed to explain the sudden appearance of this and other new spectral features at low temperature.

PACS numbers: 74.25.Kc, 74.25.Gz, 74.72.Jt

I. INTRODUCTION

Within the family of high-temperature cuprate superconductors, the Ce-doped series $R_{2-x}\text{Ce}_x\text{CuO}_{4-\delta}$, where $R=\text{Nd, Sm, Eu, Gd, etc.}$, are the only materials which appear to be electron doped.¹ The undoped Nd_2CuO_4 and Pr_2CuO_4 are antiferromagnetic insulators, which become “bad metals” with Ce doping until the sudden onset of superconductivity at $x \approx 0.14$. The region of superconductivity in the electron-doped materials is quite narrow ($x \approx 0.14 - 0.18$).^{2,3} There is essentially no “underdoped” region for the superconductivity, with the maximum value for the T_c 's of 23 K and 19 K in the Nd and Pr systems, respectively, occurring at $x \approx 0.15$. At higher dopings T_c decreases rapidly vanishing above $x \approx 0.18$. At the solubility limit ($x = 0.22$) the Nd system is metallic with no evidence of superconductivity.⁴ The optimally doped systems become superconducting only after oxygen reduction^{5,6,7} ($\delta \approx 0.01 - 0.03$), and some transport measurements suggest that both electrons and holes participate in the charge transport in the superconducting phase.^{8,9} The role played by oxygen in these materials may be more complex than in the hole-doped cuprates. It is the interesting behavior of these superconducting systems that motivates an examination of the optical properties of one of the parent compounds, Pr_2CuO_4 .

The T' structure of Pr_2CuO_4 is similar to the T structure of the hole-doped $\text{La}_{2-x}\text{Sr}_x\text{CuO}_4$; both structures are body-centered tetragonal, space group $I4/mmm$

(D_{4h}^{17}) (Ref. 10). These materials consist of two-dimensional sheets of copper-oxygen layers, which define the *a-b* planes, with the *c* axis being perpendicular to the planes. The T and T' structures differ in the location of the oxygen atoms between the copper-oxygen sheets. In the T structure the copper atoms have octahedral coordination, surrounded by four oxygen atoms in the *a-b* plane, and two apical oxygens along the *c* axis. However, in the T' structure shown in Fig. 1, the apical sites are empty and the out-of-plane oxygen atoms are not chemically bonded to the copper atoms in the planes, which, as a result, have a square coordination.¹¹ While the difference between the T and T' structures results in different Raman active modes, the same number of infrared active modes $3A_{2u} + B_{2u} + 4E_u$ are expected for each.¹¹ (The doubly degenerate E_u modes are active in the *a-b* planes, the singly degenerate A_{2u} modes are active only along the *c* axis, and the B_{2u} mode is silent.)

The strong Cu-O bonding in the *a-b* plane of this material gives rise to two-dimensional electronic and magnetic behavior. The weak out-of-plane coupling induces long range antiferromagnetic (AFM) order in the Cu spins at the relatively modest temperature of $T_{N,Cu} \approx 250-280$ K (Refs. 12,13,14), which is similar to the values of $T_{N,Cu} \approx 250-300$ K observed in Nd_2CuO_4 (Refs. 14,15), Eu_2CuO_4 (Ref. 16), and La_2CuO_4 (Refs. 17,18). The rare earth Pr ions carry localized $4f$ moments, which typically order at very low temperature. However, from symmetry considerations, the Pr moments should order below $T_{N,Cu}$ in this material.¹⁹ In fact, due to the sig-

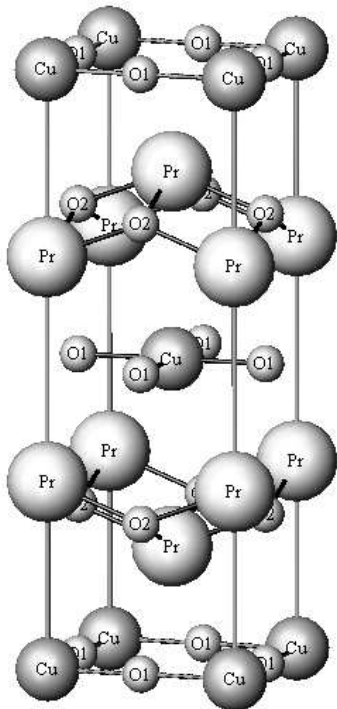


FIG. 1: The unit cell of the Pr_2CuO_4 in the $I4/mmm$ space group showing the square planar coordination of the Cu-O(1) layers, as well as the corrugated structure of the Pr-O(2) layers. The unit cell dimensions are $a = b = 3.943 \text{ \AA}$ and $c = 12.15 \text{ \AA}$ (Ref. 12).

nificant exchange interactions between the Pr ions which are mediated through the copper-oxygen layers, there is a Pr contribution to the susceptibility¹² below $\approx 200 \text{ K}$.

The optical properties of Nd_2CuO_4 have been investigated in ceramics and single crystals.^{20,21,22,23,24,25,26,27} Single crystals of Pr_2CuO_4 have been studied at either room temperature^{28,29,30,31} or at low temperature^{11,32} ($\approx 10 \text{ K}$), but there has been no detailed investigation of the temperature dependence of the optical properties of this material. Furthermore, there is some disagreement in the literature with respect to the vibrational parameters of the E_u modes.

In this paper we report on the detailed optical properties of Pr_2CuO_4 at a variety of temperatures. The conductivity at low-frequency has a strong temperature dependence above room temperature, which when taken with optical estimates of the gap suggests that the transport is due to variable-range hopping due to localized states in the gap. Transport measurements support this conclusion. A strong new vibration appears close to the low-frequency E_u mode below about 200 K , in addition to other weak vibrational structure. A normal coordinate analysis of the zone-center vibrational modes indicates that of all the E_u modes, only the low-frequency mode involves a significant Pr-Cu interaction. It is proposed that the AFM order in this material is responsible

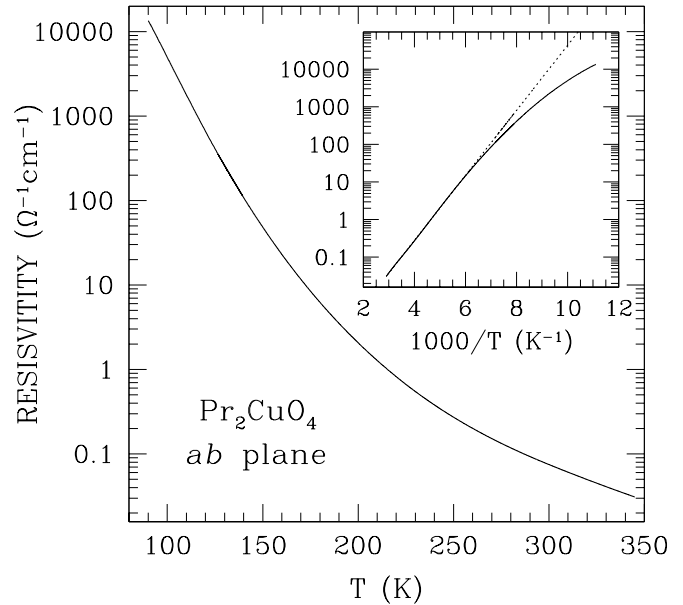


FIG. 2: The temperature dependence of the ab -plane resistivity of Pr_2CuO_4 . The resistivity is changing over nearly six orders of magnitude over the temperature interval. Inset: The resistivity vs $1/T$. This plot shows that at high temperatures the resistivity is activated and follows the form $\rho_{dc} = \rho_0 \exp(E_a/k_B T)$; a linear regression yields a value for $E_a = 1380 \pm 50 \text{ cm}^{-1}$ ($\approx 0.17 \text{ eV}$) (dotted line). Note the deviation from activated behavior at low temperature.

for the lifting of the degeneracy of the low-frequency E_u mode; the absence of any interaction between the Pr and Cu atoms in the other E_u modes limits this effect to just the low-frequency E_u mode.

II. EXPERIMENTAL

Single crystals of Pr_2CuO_4 were grown using a CuO-based direction solidification technique.³³ The crystals are thin platelets $\approx 1.5 \text{ mm} \times 1.5 \text{ mm}$ in the a - b plane, but quite thin along the c axis ($\approx 50 \mu\text{m}$). The crystals examined had a flat, mirror-like surface which was free of flux or other residue. Transport and optical measurements were performed on the same sample for consistency. The measurements of resistivity in the ab -plane were carried out using standard four-probe configuration. Gold wires were attached to the specimen directly using silver-loaded epoxy and followed by a spot annealing at the contacts with focused laser beam. The whole specimen remained at room temperature, except the areas of $\sim 70 \mu\text{m}$ wide surrounding the contacts. This process generally resulted in a contact resistance less than 1Ω . With such a low contact resistance, without changing the oxygen content in these samples, we were able to measure the resistivity over six orders of magnitude from 90 K to

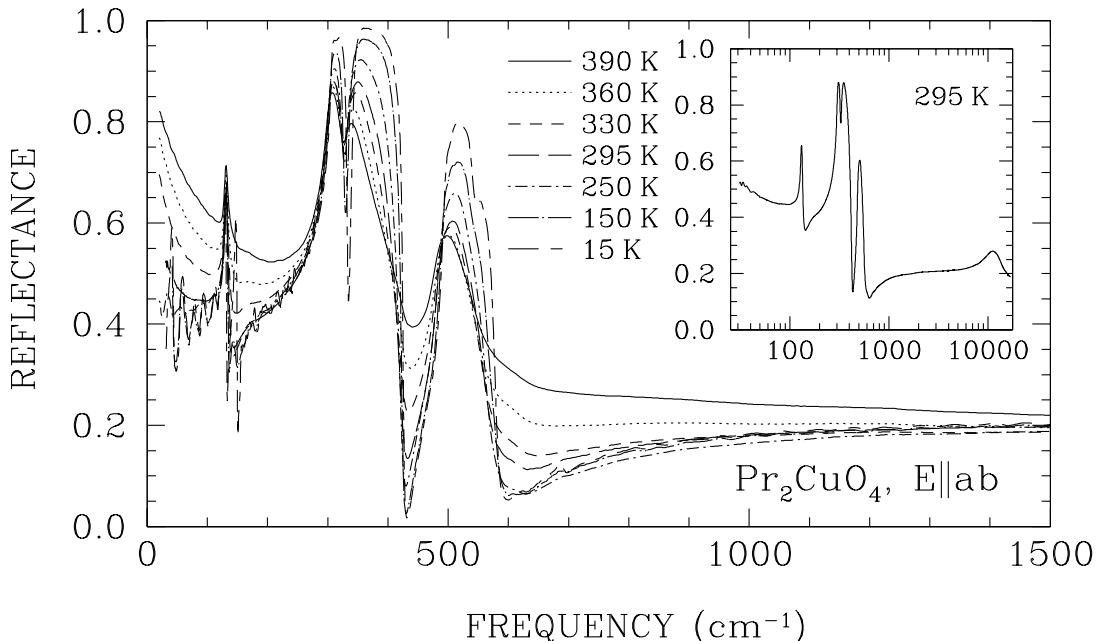


FIG. 3: The reflectance of Pr_2CuO_4 for light polarized in the a - b plane for temperatures between 15 and 390 K from ≈ 30 to 1500 cm^{-1} . Above room temperature, the low frequency reflectance goes rapidly to unity indicating a “metallic” behavior, while the rapid appearance of the low-frequency oscillatory structure at low temperature is an indication of the increasingly insulating and transparent nature of the sample. Inset: The reflectance at 295 K over a much wider frequency range from ≈ 30 to over $16\,000 \text{ cm}^{-1}$.

340 K with high accuracy (better than 0.1%), shown in Fig. 2. The inset shows the resistivity vs the inverse temperature; the linear response at high temperature is an indication of activated behavior, although this is no longer the case for $T \lesssim 160 \text{ K}$.

Magnetization measurements were performed on an unoriented 2 mg crystal of Pr_2CuO_4 in an MPMS magnetometer at an applied field of 5 T. The behavior of $1/\chi_M$ follows a Curie-Weiss form, and linear regression yields a Néel temperature for Pr of $T_{N,\text{Pr}} \approx 44 \text{ K}$ with a Pr magnetic moment of $3.2 \mu_B$. A careful survey of the temperature region in which the antiferromagnetic ordering of copper moments is expected ($200 \text{ K} < T_{N,\text{Cu}} < 320 \text{ K}$) reveals no apparent anomaly in the magnetization. A feature comparable in size and definition to that observed by Sun *et al.*¹⁷ for La_2CuO_4 would have been readily observable. However, based on the scatter in our data, an antiferromagnetic anomaly reduced in size by more than 50% and/or smeared over a larger temperature region might not be discernible. It is worth noting that the majority of studies of the ordering of the Cu spins in these materials have been neutron scattering measurements on substantially larger samples than the ones examined in this work.

For the optical measurements, crystals were mounted in a cryostat on an optically-black cone. The temperature dependence of the reflectance was measured at a near-normal angle of incidence from ≈ 30 to over $16\,000 \text{ cm}^{-1}$ on a Bruker IFS 66v/S using an *in situ* overcoating technique, which has previously been described in de-

tail elsewhere.³⁴ This technique is especially useful when measuring small samples, as it allows the entire face of the sample to be utilized. Above $\approx 5000 \text{ cm}^{-1}$ the reflectance is assumed to be temperature independent.

The optical conductivity has been determined from a Kramers-Kronig analysis of the reflectance, for which extrapolations to $\omega \rightarrow 0, \infty$ must be supplied. At low frequency, a metallic extrapolation was used for $T \gtrsim 260 \text{ K}$, $R \propto 1 - \sqrt{\omega}$; while below this temperature the reflectance was assumed to continue smoothly to ≈ 0.45 at zero frequency. At high frequency, the reflectance was assumed to be constant above the highest measured frequency point to $2 \times 10^5 \text{ cm}^{-1}$, above which a free-electron ($R \propto \omega^{-4}$) behavior was assumed. At low temperature, the semitransparent nature of the sample has implications for the Kramers-Kronig analysis, which assumes specular reflectance from a single surface only. While the absorption due to the lattice modes assures that the reflectance in those regions is essentially that of the bulk material, the same cannot be said for the high-frequency region. The presence of multiple reflections leads to asymmetries in the line shapes and an optical conductivity less than zero. As a result, for the calculation of the low-frequency conductivity in the region of the lattice modes, the reflectance has been truncated at $\approx 3000 \text{ cm}^{-1}$ and assumed to be constant only to 8000 cm^{-1} , above which a free electron approximation has been assumed. While the lineshapes in the conductivity are symmetric Lorentzians whose positions and widths do not vary greatly with different choices for the

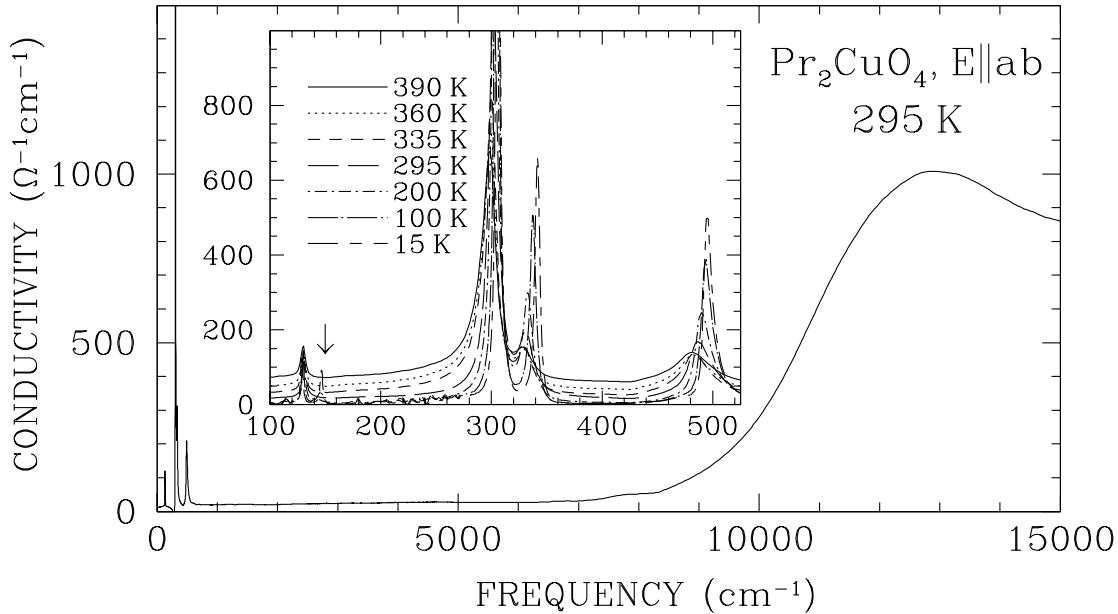


FIG. 4: The optical conductivity of Pr_2CuO_4 from ≈ 30 to $16\,000\text{ cm}^{-1}$ at 295 K for light polarized in the a - b plane. Inset: the temperature dependence of the conductivity in the region of the four infrared-active E_u modes; while the conductivity is dominated by the lattice vibrations, a broad incoherent background is observed to form rapidly above room temperature. Note also the appearance of a new low-frequency vibrational feature at low temperature at $\approx 145\text{ cm}^{-1}$ (arrow).

high-frequency extrapolations, the amplitudes are somewhat sensitive upon this choice.

III. RESULTS

The reflectance of Pr_2CuO_4 for light polarized in the a - b plane is shown in Fig. 3 from ≈ 20 to 1500 cm^{-1} at a variety of temperatures, and in the inset from ≈ 30 to $16\,000\text{ cm}^{-1}$ at room temperature. The reflectance at low frequency is dominated by structure due to the normally-active infrared modes, while the reflectance at high frequency is relatively featureless, except for some structure at $\approx 11\,000\text{ cm}^{-1}$. The low-frequency vibration at $\approx 130\text{ cm}^{-1}$ is observed to be a single mode at room temperature. However, at low temperature this mode is resolved as a doublet. The low-frequency reflectance has an interesting behavior; at low temperature the fringes indicate a lack of absorption due to the insulating nature of the sample, but at room temperature and above the fringes have vanished and the reflectance appears to be tending towards unity as $\omega \rightarrow 0$; at 390 K the low frequency reflectance is over 80% and the system appears to be weakly metallic.

The optical conductivity $\sigma_1(\omega)$ calculated from a Kramers-Kronig analysis of the reflectance at 295 K is shown in Fig. 4. The low frequency conductivity is dominated by the infrared-active E_u lattice modes, but a careful examination shows a slight asymmetry in the line-shape of the strongest mode. The weak feature in ob-

served in the reflectance at $\approx 11\,000\text{ cm}^{-1}$ signals the onset of absorption in the conductivity at about 9000 cm^{-1} , which peaks at about $12\,000\text{ cm}^{-1}$. The optical conductivity in the region of the infrared active modes calculated using the truncated reflectance is shown in the inset of Fig. 3. The modes have symmetric profiles, and the three high-frequency modes all harden and narrow with decreasing frequency.

The low frequency conductivity is shown in detail in Fig. 5 from ≈ 20 to 180 cm^{-1} . At 390 K , there is a considerable amount of background conductivity ($\approx 75\text{ }\Omega^{-1}\text{cm}^{-1}$) over most of the observed frequency range, which decreases rapidly with decreasing temperature. The inset in Fig. 5 shows the extrapolated value of the resistivity $\rho_{dc} \approx 1/\sigma_1(\omega \rightarrow 0)$ vs $1/T$ ($T \gtrsim 250\text{ K}$); the linear behavior indicates that the conductivity is strongly activated.³⁵

The behavior of the low-frequency mode is seen clearly in a more detailed plot of the ab -plane reflectance shown in Fig. 6 and the conductivity in upper inset. The low-frequency mode can now clearly be distinguished as fundamental at $\approx 130\text{ cm}^{-1}$. A new feature appears quickly below room temperature, gaining oscillator strength monotonically with decreasing temperature and hardening to $\approx 145\text{ cm}^{-1}$ at low temperature.

The slightly transparent nature of the sample requires that the reflections from the back of the crystal be considered. This approach is described in Appendix A, and the results of fits to the reflectance using this method are listed in Table I.

TABLE I: The results of fitting the phonon parameters to the reflectance of Pr_2CuO_4 for light polarized in the a - b plane at 295, 200 and 15 K, using the model for a lamellar plate.³⁶ A thickness of $d = 50 \mu\text{m}$ and $\epsilon_\infty = 6.5$ have been assumed. The parameters $\omega_{TO,i}$, γ_i and $\omega_{p,i}$ refer to the frequency, width and effective plasma frequency of the i th vibration. [All units are in cm^{-1} , except for the dimensionless oscillator strength $S_i = \omega_{p,i}^2/\omega_{TO,i}^2$.]

295 K				200 K				15 K			
$\omega_{TO,i}$	γ_i	$\omega_{p,i}$	(S_i)	$\omega_{TO,i}$	γ_i	$\omega_{p,i}$	(S_i)	$\omega_{TO,i}$	γ_i	$\omega_{p,i}$	(S_i)
130.6	4.5	161	(1.51)	130.4	3.3	157	(1.45)	128.2	2.7	144	(1.26)
					141.1	9.9	69		(0.24)	146.1	2.4
304	7.5	815	(7.18)	305	3.0	831	(7.42)	306	1.4	834	(7.43)
331	17.4	469	(2.01)	333	7.7	458	(1.89)	341	3.4	431	(1.59)
490	27.3	511	(1.08)	491	19.5	508	(1.07)	495	8.4	503	(1.03)
				541	38	112	(0.04)	542	25	108	(0.04)
				688	25	60	(0.01)	688	15	90	(0.02)

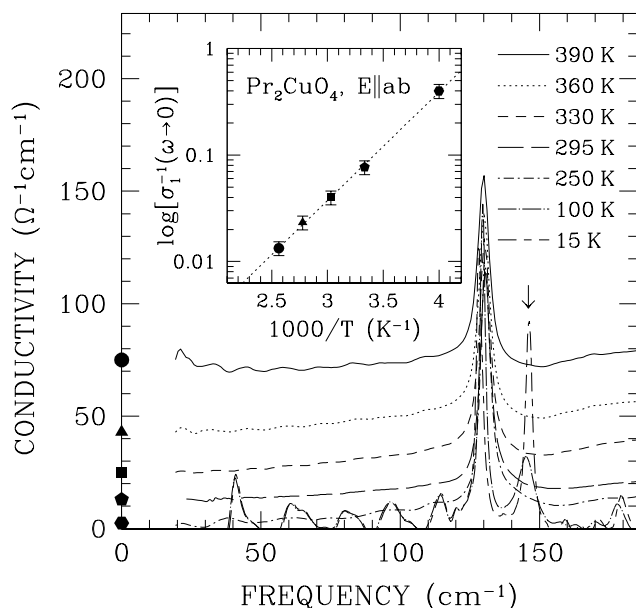


FIG. 5: The optical conductivity of Pr_2CuO_4 at low frequency for light polarized in the a - b plane from 15 to 390 K showing the rapid formation of the background conductivity, and the extrapolated values for $\rho_{dc} = 1/\sigma_1(\omega \rightarrow 0)$; the different symbols denote the extrapolated values at different temperatures. At low temperature a strong new vibrational feature is observed (arrow). Inset: the extrapolated values for ρ_{dc} vs $1/T$; the linear regression of the points (dotted line) yields $E_a = 1630 \pm 200 \text{ cm}^{-1}$ ($\approx 0.2 \text{ eV}$).

IV. DISCUSSION

A. Electronic properties

The peak in the optical conductivity of Pr_2CuO_4 at $\approx 12500 \text{ cm}^{-1}$ in Fig. 4 has been observed in previous work.^{23,28,30} The location of this feature is similar to the onset of absorption in La_2CuO_4 and related materials³⁷ at $\approx 11000 \text{ cm}^{-1}$ ($\approx 1.4 \text{ eV}$). The peak is characteristic

of a semiconducting band edge or a polaronic excitation. In either of these cases, the dc resistivity is expected to be activated and to follow the form³⁸

$$\rho_{dc} \propto e^{E_a/k_B T}, \quad (1)$$

where E_a is either the half the optical gap 2Δ , or half the polaronic level shift E_p . The low-frequency reflectance increases quickly above room temperature, which is indicative of a “metallic” response in which the reflectance goes to unity at zero frequency. This observation is realized in the optical conductivity, where $\sigma_{dc} \equiv \sigma_1(\omega \rightarrow 0)$ has a very strong temperature dependence for $T \gtrsim 300 \text{ K}$. The plot of $\rho_{dc} = 1/\sigma_{dc}$ vs $1/T$ is shown in the inset in Fig. 5, and is described quite well by Eq. (1); a linear regression yields $E_a \approx 1630 \pm 200 \text{ cm}^{-1}$ ($\approx 0.2 \text{ eV}$). The rather large error associated with this estimate is due to the fact that the fit is limited to a narrow interval in the high-temperature region. The transport data shown in Fig. 2 and the inset are also described quite well by activated behavior; a linear regression applied in the high-temperature region ($T \gtrsim 160 \text{ K}$) yields $E_a = 1380 \pm 50 \text{ cm}^{-1}$ ($\approx 0.17 \text{ eV}$) and is shown as a dashed line in the inset of Fig. 2; this value for E_a is fairly close to the value determined from the optical conductivity. The optical conductivity of the nickelates, which have a similar appearance, has been fitted using a small-polaron model,^{38,39,40} which for $T \gg \omega/2$ produces an asymmetric Gaussian peak with a maximum at $4E_a$. This model would imply that the peak in the conductivity at high temperature should occur at $\approx 6000 \text{ cm}^{-1}$, which is much less than the observed value of $\approx 12500 \text{ cm}^{-1}$. A rough estimate of the direct optical gap may be made by extrapolating from the linear part of the leading edge conductivity in Fig. 4 to the abscissa, which gives $2\Delta \approx 9500 \text{ cm}^{-1}$. If the transport were due to the carrier pair density from thermal excitations across the gap, then $\sigma_{dc} \propto n_i \approx \exp(-\Delta/k_B T)$. However, $E_a \ll \Delta$, suggesting that the dc transport is due to variable range hopping between localized states within the gap.⁴¹ At low temperatures, the resistivity due to hopping is not activated, but instead has the form

$$\rho_{dc} \propto e^{(T_0/T)^{1/n}}, \quad (2)$$

B. Vibrational properties

1. Normal coordinate analysis of the lattice modes

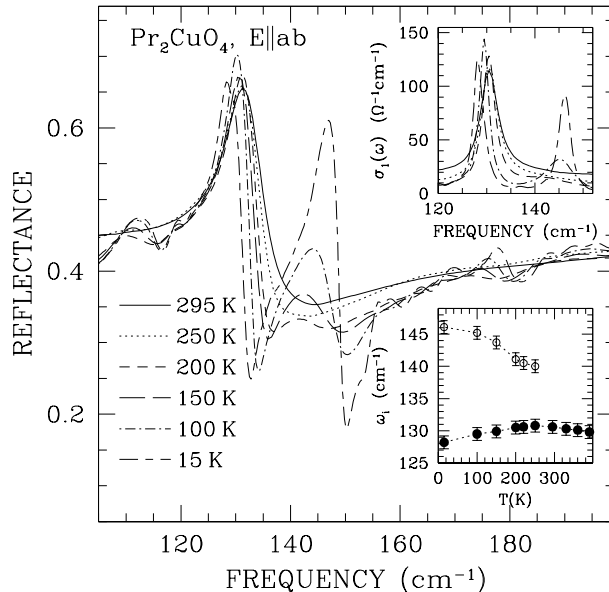


FIG. 6: The reflectance of Pr_2CuO_4 for light polarized in the a - b planes in the region of the low frequency infrared-active E_u mode. The vibration is a single mode at room temperature, but is resolved as a doublet at low temperature. Upper inset: The optical conductivity which shows not only the appearance of the new mode, but also the rapid increase in strength and narrowing of this feature. Lower inset: The temperature dependence of the fundamental mode (filled circles) and the new vibrational feature (open circles).

where T_0 is a characteristic temperature, and $n = d + 1$ and d is the dimensionality of the system.⁴¹ The transport measurements have been performed over a wide enough range so that the departure from activated to power-law behavior at low temperature is clearly visible in the insert in Fig. 2. Different power laws were examined, but it appears that the resistivity at low temperature is well described by $\rho_{dc} \propto \exp[(T_0/T)^{1/4}]$, suggesting that the hopping is a three-dimensional rather than a two-dimensional phenomena restricted to the CuO_2 planes.⁴² The localized states that result in hopping may arise from defects which produced states within the gap. There is a very weak feature in the optical conductivity in Fig. 4 at $\approx 8000 \text{ cm}^{-1}$ which occurs at $\approx E_a$ below the leading edge of the absorption. This feature may suggest a possible origin for the localized states. However, it not clear if the defects states responsible for this feature are an intrinsic property of the sample, or due to extrinsic effects.

The unusual behavior of the low-frequency E_u mode requires a detailed understanding not only of the nature of this particular mode, but of the other E_u modes as well. For this reason, a normal coordinate analysis of Pr_2CuO_4 was undertaken.⁴³

The normal coordinate calculations were performed using Wilson's GF matrix method^{44,45} and a commercially available software package.⁴⁶ Initially, a simple valence force field was adopted, consisting of bond stretching and angle bending coordinates; the types and values of the force constants used, and the internal coordinates to which they correspond are listed in Table II. The force field involves six bond stretching force constants and four angle bending force constants. The bond stretch and angle bends all involve oxygen bonding, with the exception of the bond stretches denoted f_4 and f_6 , which deal with the Pr-Pr and Pr-Cu interactions; while the value for the Pr-Cu bond stretch is relatively small, the refinement is significantly worse if it is omitted. While this initial force field described the vibrations in the Cu-O(1) planes quite well, the corrugated nature of the Pr-O(2) layers shown in Fig. 1 leads to difficulties in describing the restoring forces within this layer. The agreement with the observed frequencies improved significantly when an interaction force constant between the bond stretch and the angle bend in the Pr-O(2) layer was introduced. The comparison between observed and calculated frequencies, and the potential energy distribution (PED) are listed in Table III. The PED's gives the relative contribution of the force constants to the potential energy of the normal modes. This treatment yields the atomic displacements and PED for all of the normal modes. Each of the in-plane infrared active E_u modes merits further discussion.

The E_u mode at 490 cm^{-1} at room temperature involves primarily the in-plane Cu-O angle bending resulting in displacements of the O(1) atoms. In addition, there are small displacements of the atoms in the Pr-O(2) planes; the motions of the Pr and O(1) atoms are coordinated. However, as Table III shows, there is no interaction between the rather small Pr and the Cu displacements. In general, the eigenvectors determined from the normal coordinate analysis are in good agreement with the calculated zone-center displacements shown in Ref. 22. This mode hardens to 495 cm^{-1} at 15 K and narrows dramatically from ≈ 25 to $\approx 8 \text{ cm}^{-1}$, as shown in Table I. The oscillator strength of this mode does not vary with temperature. The slight asymmetry that is observed in the optical conductivity of the high-frequency E_u mode in Fig. 4 is most likely produced by the uncertainty in the high-frequency extrapolation used in the Kramers-Kronig analysis; fits to the reflectance are exact and do not suggest a large asymmetry in this feature or others (Appendix A).

The mode at 331 cm^{-1} is a pure Pr-O(2) bond stretch,

TABLE II: Force constants and internal coordinates for Pr_2CuO_4 . The labeling scheme of the atoms is shown in Fig. 1.

Force constant	Internal coordinate		Distance (\AA)/ Angle ($^\circ$)	Value ^a
Bond stretch				
f_1	Cu-O(1)	[4] ^b	1.98	0.355
f_2	Pr-O(2)	[8]	2.12	0.532
f_3	Pr-O(1)	[8]	3.03	0.785
f_4	Pr-Pr	[1]	4.58	0.787
f_5	O(2)-O(2)	[4]	2.80	0.300
f_6	Pr-Cu	[8]	3.62	0.067
Angle bend				
α_1	O(1)-Cu-O(1)	[4]	90	0.572
α_2	O(1)-Cu-O(1) ^c	[4]	180	0.195
α_3	O(2)-Pr-O(2)	[4]	138	0.469
α_4	O(1)-Pr-O(1)	[4]	82	0.478
Interaction				
i_1	$f_2\alpha_3$	[16]		0.074

^aBond stretches are in units of $\text{md}/\text{\AA}$, angle bends in $\text{md}\cdot\text{\AA}/\text{rad}$.

^bThe number of internal coordinates.

^cIn plane and out of plane.

while the 304 cm^{-1} mode is almost a pure Cu-O(1) bond stretch (Table III). The mode at 331 cm^{-1} hardens considerably to 341 cm^{-1} at 15 K, and also narrows from ≈ 17 to 3.4 cm^{-1} . The mode at $\approx 304\text{ cm}^{-1}$ hardens only slightly with decreasing temperature, but narrows significantly from $\approx 8\text{ cm}^{-1}$ at room temperature to 1.4 cm^{-1} at 15 K; this is the strongest E_u mode with an oscillator strength of $S \approx 7.4$.

The mode at 130 cm^{-1} is a combination of Cu-O angle bending, resulting in the in-plane displacements of the Cu and O(1) atoms, as well as the out-of-phase motion of the Pr and O(2) atoms in the Pr-O layers; interestingly, this mode has a significant coordination between the displacements of the Pr atoms and the Cu and O(1) atoms, indicated in Table III. The only other mode that has a strong Pr-Cu interaction is the low-frequency c -axis A_{2u} mode. The low-frequency E_u mode softens to $\approx 128\text{ cm}^{-1}$ at low temperature, while narrowing. The observed frequencies are in good agreement with previous work,^{29,32} however, the linewidths are all narrower and there is only rough agreement with the reported strengths.

2. Origin of the low temperature doublet at $\approx 130\text{ cm}^{-1}$

The most unusual feature in the reflectance spectra is striking appearance of a new mode at low temperature, which is just above the low frequency E_u mode. The new mode is not simply a peculiar artifact due to fringes in the presence of vibrational structure, as Fig. 7(b) demonstrates (Appendix A). While this feature has been previously observed at low temperature^{11,32} the evolution of

this new mode has never been studied or fully explained. The new feature appears suddenly below $\lesssim 250\text{ K}$ at $\approx 140\text{ cm}^{-1}$, as seen in Fig. 6 and in the insets; this mode hardens dramatically and narrows with decreasing temperature, gaining strength monotonically until it has almost the same oscillator strength as the low-frequency E_u mode (Table I). This feature does not appear to evolve from a strong asymmetry or shoulder in the low-frequency E_u mode. There is also additional very weak new fine structure in the low temperature reflectance at ≈ 541 and 688 cm^{-1} . These frequencies are well above the high-frequency E_u mode at $\approx 490\text{ cm}^{-1}$. A symmetry-breaking process would allow Raman-active modes as well as the longitudinal optic (LO) modes to become weakly active. However, the highest observed frequency for a Raman mode is the E_g mode at $\approx 480\text{ cm}^{-1}$, suggesting that these features are not Raman modes. To determine the positions of the LO modes, the reflectance and optical conductivity have also been fit using a factorized form of the dielectric function⁴⁷

$$\tilde{\epsilon}(\omega) = \epsilon_\infty \prod_j \frac{\omega_{LO,j}^2 - \omega^2 - i\gamma_{LO,j}\omega}{\omega_{TO,j}^2 - \omega^2 - i\gamma_{TO,j}\omega}, \quad (3)$$

where $\omega_{LO,j}$, $\omega_{TO,j}$, $\gamma_{LO,j}$ and $\gamma_{TO,j}$ are the j th LO and the normally-active transverse optic (TO) modes, and LO and TO damping, respectively. The fit at 15 K yields values for the TO modes which are nearly identical to those shown in Table I, and LO modes at 131, 149, 332, 430 and 588 cm^{-1} , respectively. None of the LO modes are close to the new features observed at low temperature, making it unlikely that any new structure is due to the LO modes.

A more promising explanation of the splitting of the low frequency mode may involve the fact that of all the E_u modes, only the low-frequency mode involves a significant Pr-Cu interaction. Magnetization measurements in this work show that the Pr atoms are ordered at low temperature ($\lesssim 50\text{ K}$), and neutron scattering measurements¹² show that there is at least a partial ordering at higher temperatures, indicating the presence of a Pr-Cu exchange interaction. In the case of the low-frequency E_u mode, the displacements of the Pr and Cu atoms are strongly correlated, suggesting that the exchange interaction will have a significant effect upon the nature of this vibration. This can lead to a symmetry-breaking process and the splitting of the doubly-degenerate E_u mode. This view is consistent with the observation that this new feature is *not* present in $\text{Pr}_{1.85}\text{Ce}_{0.15}\text{CuO}_4$, which is in the region of the phase diagram for this class of materials where the AFM order is destroyed.²¹ Because the other E_u modes do not involve strong Pr-Cu coupling, no exchange-induced splitting would be expected. In fact, of all the other vibrational modes, only the low-frequency A_{2u} mode has a significant Pr-Cu interaction (Table III), but since this mode is singly degenerate no splitting is expected, nor it is observed.³² Similar behavior might also be expected in Nd_2CuO_4 , where the Nd moments order below 37 K.

TABLE III: Calculated and observed frequencies for the zone-center vibrations of Pr_2CuO_4 at room temperature, and the potential energy distribution (PED). (All frequencies are in cm^{-1} .)

Symmetry	obs. ^a	cal.	PED ^b ($\geq 10\%$)
A_{1g}	228	227	$f_3(42), f_4(37), \alpha_3(17)$
B_{1g}	328	326	$f_2(28), \alpha_3(73)$
E_g	480	481	$f_2(46), f_5(54)$
E_g	126	123	$f_2(18), f_3(52), f_5(23)$
A_{2u}	505	504	$f_3(83)$
A_{2u}	271	271	$f_2(43), \alpha_3(113), i_1(-58)$
A_{2u}	135	135	$f_6(37), \alpha_2(58)$
B_{2u}	(silent)	480	$f_3(82)$
E_u	490	490	$f_3(60), \alpha_1(29), \alpha_2(10)$
E_u	331	332	$f_2(98)$
E_u	304	303	$f_1(93)$
E_u	131	129	$f_3(28), f_6(22), \alpha_1(30), \alpha_2(10)$

^aThe observed frequencies for the A_{2u} modes are taken from Ref. 29, while the Raman active modes are taken as those for Nd_2CuO_4 from Ref. 49. The frequencies for the E_u modes are from this work (Table I).

^bSee Table II for the identification of the force constants.

In fact, a weak feature is observed in the reflectance of Nd_2CuO_4 at 10 K at $\approx 165 \text{ cm}^{-1}$, quite close to the low-frequency E_u mode, and it has been suggested that this feature is indeed magnetic in origin.²¹ Kramers doublets have also been reported in the Raman spectra at low temperature,⁴⁸ which have been attributed to the removal of degeneracy by the Nd-Cu exchange interaction.⁴⁹ While this is a reasonable explanation for the strong feature at low frequency, it is less satisfactory for the fine structure observed at high frequency.

The new structure observed at $\approx 688 \text{ cm}^{-1}$ at low temperature is similar in frequency to structure that has been observed the reflectance in other electron-doped materials^{27,50} at $\approx 690 \text{ cm}^{-1}$. It has been suggested that much of the fine structure observed in the cuprate systems are local vibrational modes due to polaron fine structure.^{27,51} Alternatively, a number of weak features are also seen below the Néel transition in CuO , including a mode at $\approx 690 \text{ cm}^{-1}$, which has been attributed to the activation of a zone-boundary mode due to the reduction of the Brillouin zone resulting from the magnetic order.^{52,53} It is possible that the magnetic order is responsible for a weak structural distortion and the activation of zone boundary modes due to the commensurate reduction of the Brillouin zone. However, a difficulty with this explanation is that any reduction of the Brillouin zone should result in a many new modes being activated, rather than just the three that are observed. One of the difficulties in explaining the vibrational fine structure observed in this system is the failure to observe these results on a consistent basis in different studies.^{27,54} This raises the distinct possibility that some of these features arise from impurities and/or phase separation, ultimately making it difficult to identify a specific mechanism

responsible for the origin of the fine structure.

V. CONCLUSIONS

The strong temperature dependence of the low-frequency reflectance above $\approx 250 \text{ K}$ results in a resistivity $\rho_{dc} \approx 1/\sigma_1(\omega \rightarrow 0)$ which is exponential with temperature, following the functional form $\rho_{dc} \propto \exp(E_a/k_B T)$, where $E_a \approx 0.20 \text{ eV}$; a more detailed transport measurement yields a slightly lower and more accurate value of $E_a \approx 0.17 \text{ eV}$. The fact that the transport gap E_a is much less than the inferred optical gap $2\Delta \approx 1.2 \text{ eV}$, and that transport measurements of the resistivity show a departure from activated behavior for $T \lesssim 160 \text{ K}$ to a $\rho_{dc} \propto \exp[(T_0/T)^{1/4}]$ power-law behavior suggests that the transport in this material is due to variable-range hopping between localized states in the gap.

Due to the unusual vibrational structure in Pr_2CuO_4 at low temperature, considerable attention was devoted to a discussion of the lattice modes. A normal coordinate analysis has been performed to provide a detailed understanding of the nature of the zone-center vibrations in this material. A prominent feature close to the low-frequency E_u mode develops at low temperature, and additional weak fine structure is observed at high frequency. These new features appear below $T_{N,Cu}$ at roughly the same temperature at which the Pr moments are thought to begin to order ($\approx 200 \text{ K}$). Only the low-frequency E_u mode involves a significant Pr-Cu interaction. This suggests that the new vibrational structure is due to the antiferromagnetic order in this material and the removal of degeneracy of this mode.

Acknowledgments

We are grateful to A.R. Moodenbaugh for performing the magnetization measurements. We would also like to thank D.N. Basov, V.J. Emery, J.L. Musfeldt, M. Strongin, T. Timusk, J.M. Tranquada, and J.J. Tu for many helpful discussions. This work was supported by the Department of Energy under contract number DE-AC02-98CH10886; work in Maryland is supported by the NSF Condensed Matter Physics Division under grant No. DMR 9732736. Research undertaken at NSLS was supported by the U.S. DOE, Division of Materials and Chemical Sciences.

APPENDIX A: REFLECTANCE OF A DIELECTRIC SLAB

Due to the complications introduced by the slightly transparent nature of the sample, the reflectance and the lattice modes have been fit using a model which considers reflections from both the front and back surfaces of the

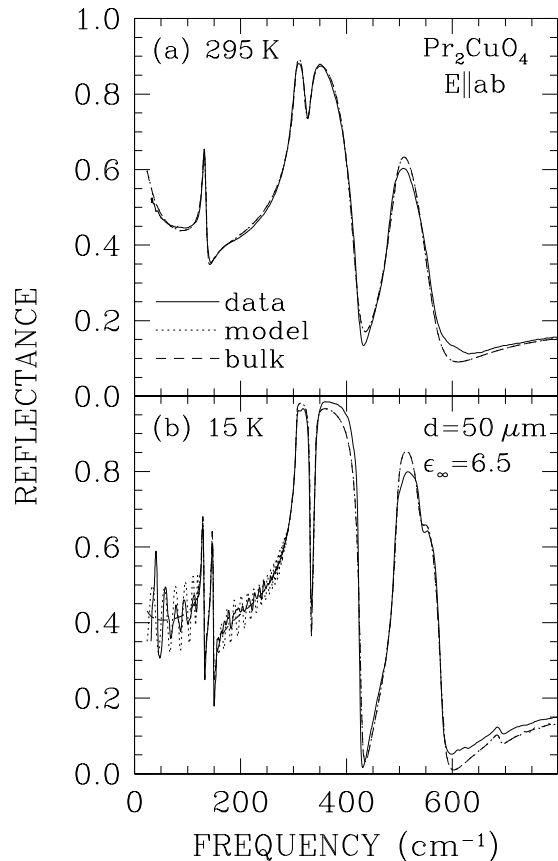


FIG. 7: (a) The reflectance in the infrared region of Pr_2CuO_4 for light polarized in the a - b plane at room temperature (solid line) and the fit to the data from Eq. (1) (dotted line) using the vibrational parameters in Table I, with $\epsilon_\infty = 6.5$ and a sample thickness of $d = 50 \mu\text{m}$. The dashed line indicates the calculated behavior the (infinitely thick) bulk material, which is identical to that of the model, indicating the opaque nature of the sample. (b) The reflectance at 15 K (solid line) with the model fit (dotted line) using the vibrational parameters in Table I, using the same values for d and ϵ_∞ . The dashed line indicates the calculated behavior of the bulk material. The doublet structure, fringe spacing and amplitude are in good agreement with the reflectance. Note the absence of fringes in regions of strong absorption.

crystal. The frequency-dependent reflectance of a lamellar plate at a normal angle of incidence is $R = \tilde{r}_l \tilde{r}_l^*$, where \tilde{r}_l is defined as

$$\tilde{r}_l = \frac{\tilde{r} [1 - e^{i\omega 4\pi \tilde{n} d}]}{1 - r^2 e^{i\omega 4\pi \tilde{n} d}}, \quad (\text{A1})$$

where d is the sample thickness, and \tilde{r} is the Fresnel reflectance of the bulk material,

$$\tilde{r} = \frac{1 - \tilde{n}}{1 + \tilde{n}}. \quad (\text{A2})$$

The complex refractive index is $\tilde{n} = n + ik$, which is related to the complex dielectric function $\tilde{\epsilon} = \epsilon_1 + i\epsilon_2 = \tilde{n}^2$, allowing the real and imaginary parts of the refractive index n and k to be determined

$$n = \left\{ \frac{1}{2} \left[\sqrt{\epsilon_1^2 + \epsilon_2^2} + \epsilon_1 \right] \right\}^{1/2}, \quad (\text{A3})$$

$$k = \left\{ \frac{1}{2} \left[\sqrt{\epsilon_1^2 + \epsilon_2^2} - \epsilon_1 \right] \right\}^{1/2}. \quad (\text{A4})$$

The optical properties of the bulk material are modeled using a series of Lorentzian oscillators

$$\tilde{\epsilon}(\omega) = \epsilon_\infty + \sum_j \frac{\omega_{p,j}^2}{\omega_j^2 - \omega^2 - i\gamma_j \omega}, \quad (\text{A5})$$

where ω_j , γ_j and $\omega_{p,j}$ are the frequency, width and effective plasma frequency of the j th vibration, and ϵ_∞ is the core contribution to the dielectric function. The dimensionless oscillator strength is written as $S_j = \omega_{p,j}^2 / \omega_j^2$. The optical conductivity $\tilde{\sigma}(\omega) = \sigma_1(\omega) + i\sigma_2(\omega)$ is related to the complex dielectric function by $\tilde{\sigma}(\omega) = -i\omega \tilde{\epsilon}(\omega) / 4\pi$.

The phonon parameters were refined by a non-linear least-squares fit of the model for the reflectance of a thin dielectric slab to the experimental reflectance in Fig. 3. The results at 295, 200 and 15 K are listed in Table I, and a comparison of the experimental reflectance and the model results are shown in Figs. 7(a) and 7(b) at 295 and 15 K, respectively. The broad, incoherent electronic background observed at room temperature is modeled by a zero-frequency Drude term, as well as two mid-infrared overdamped oscillators (Table I). The results were then compared with fits to the features in the conductivity by assuming simple linear background in the region of the lattice modes, and were found to be in good agreement. This indicates that in the region of the phonon features where the sample is opaque, the Kramers-Kronig relation yields acceptable values for the conductivity.

* Electronic address: homes@bnl.gov

† Present address: Département de Physique, Université de Sherbrooke, Sherbrooke, Québec, J1K 2R1 Canada.

¹ Y. Tokura and S. Uchida, Nature (London) **377**, 345 (1989).

² H. Takagi, S. Uchida, and Y. Tokura, Phys. Rev. Lett. **62**,

- 1197 (1989).
- ³ H. Takagi, Y. Tokura, and S. Uchida, *Physica C* **162-164**, 1101 (1989).
 - ⁴ S. J. Hagen, J. L. Peng, X. Y. Li, , and R. L. Greene, *Phys. Rev. B* **43**, 13606 (1991).
 - ⁵ F. Izumi, Y. Matui, H. Takagi, S. Uchida, Y. Tokura, and H. Assano, *Physica C* **158**, 433 (1989).
 - ⁶ P. W. Klamut, *J. Alloys Comp.* **194**, L5 (1993).
 - ⁷ T. Kawashima and E. Takayama-Mouromachi, *Physica C* **219**, 389 (1994).
 - ⁸ W. Jiang, S. N. Mao, X. X. Xi, X. Jiang, J. L. Peng, T. Venkatesan, C. J. Lobb, and R. L. Greene, *Phys. Rev. Lett.* **73**, 1291 (1994).
 - ⁹ P. Fournier, X. Jiang, W. Jiang, S. N. Mao, T. Venkatesan, C. J. Lobb, and R. L. Greene, *Phys. Rev. B* **56**, 14149 (1997).
 - ¹⁰ H. Müller-Buschbaum and W. Wollschläger, *Z. Anorg. Allg. Chem.* **414**, 76 (1975).
 - ¹¹ M. K. Crawford, G. Burns, G. V. Chandrashekhar, F. H. Dacol, W. E. Farneth, E. M. McCarron, III, and R. J. Smalley, *Phys. Rev. B* **41**, 8933 (1990).
 - ¹² J. W. Sumarlin, J. W. Lynn, T. Chattopadhyay, S. N. Barilo, D. I. Zhigunov, and J. L. Peng, *Phys. Rev. B* **51**, 5824 (1995).
 - ¹³ D. E. Cox, A. I. Godman, M. A. Subramanian, J. Gopalakrishnan, and A. W. Sleight, *Phys. Rev. B* **40**, 6998 (1989).
 - ¹⁴ M. Matsuda, K. Yamada, K. Kakurai, H. Kadowaki, T. R. Thurston, Y. Endoh, Y. Hidaka, R. Birgeneau, M. A. Kastner, P. M. Gehring, et al., *Phys. Rev. B* **42**, 10098 (1990).
 - ¹⁵ Y. Endoh, M. Matsuda, K. Yamada, K. Kakurai, Y. Hidaka, G. Shirane, and R. J. Birgeneau, *Phys. Rev. B* **40**, 7023 (1989).
 - ¹⁶ T. Chattopadhyay, J. W. Lynn, N. Rosov, T. E. Greigereit, S. N. Barilo, and D. I. Zhigunov, *Phys. Rev. B* **49**, 9944 (1994).
 - ¹⁷ K. Sun, J. H. Cho, F. C. Chou, W. C. Lee, L. L. Smith, D. C. Johnston, Y. Hidaka, and T. Murakami, *Phys. Rev. B* **43**, 239 (1991).
 - ¹⁸ S. M. Hayden, G. Aeppli, R. Osborn, A. D. Taylor, T. Perring, S.-W. Cheong, and Z. Fisk, *Phys. Rev. Lett.* **67**, 3622 (1991).
 - ¹⁹ J. P. Hill, A. Vigliante, D. Gibbs, J. L. Peng, and R. L. Greene, *Phys. Rev. B* **52**, 6575 (1995).
 - ²⁰ L. Degiorgi, S. Rusiecki, and P. Wachter, *Physica C* **161**, 239 (1989).
 - ²¹ E. T. Heyen, G. Kliche, W. Kress, W. König, M. Cardona, E. Rampf, J. Prade, U. Schröder, A. D. Kulkarni, F. W. de Wette, et al., *Solid State Commun.* **74**, 1299 (1990).
 - ²² J.-G. Zhang, X.-X. Bi, E. McRae, P. C. Eklund, B. C. Sales, and M. Mostoller, *Phys. Rev. B* **43**, 5389 (1991).
 - ²³ S. Lupi, P. Calvani, M. Capizzi, P. Maselli, W. Sadowski, and E. Walker, *Phys. Rev. B* **45**, 12470 (1992).
 - ²⁴ S. Jandl, P. Dufour, T. Strach, T. Ruf, M. Cardona, V. Nekvasil, C. Chen, and B. M. Wanklyn, *Phys. Rev. B* **52**, 15558 (1995).
 - ²⁵ S. Jandl, P. Dufour, T. Strach, T. Ruf, M. Cardona, V. Nekvasil, C. Chen, B. M. Wanklyn, and S. Piñol, *Phys. Rev. B* **53**, 8632 (1996).
 - ²⁶ T. Strach, T. Ruf, M. Cardona, S. Jandl, V. Nekvasil, C. Chen, B. M. Wanklyn, D. I. Zhigunov, S. N. Barilo, and S. V. Shiryaev, *Phys. Rev. B* **56**, 5578 (1997).
 - ²⁷ P. Calvani, M. Capizzi, S. Lupi, P. Maselli, A. Paolone, and P. Roy, *Phys. Rev. B* **53**, 2756 (1996).
 - ²⁸ S. L. Cooper, G. A. Thomas, J. Orenstein, D. H. Rapkine, A. J. Millis, S.-W. Cheong, A. S. Cooper, and Z. Fisk, *Phys. Rev. B* **41**, 11605 (1990).
 - ²⁹ S. Tajima, T. Ido, S. Ishibashi, T. Itoh, H. Eisaki, Y. Mizuo, T. Arima, H. Takagi, and S. Uchida, *Phys. Rev. B* **43**, 10496 (1991).
 - ³⁰ T. Arima, Y. Tokura, and S. Uchida, *Phys. Rev. B* **48**, 6597 (1993).
 - ³¹ S. Jandl, T. Strach, T. Ruf, M. Cardona, V. Nekvasil, M. Iliev, D. I. Zhigunov, S. N. Barilo, and S. V. Shiryaev, *Phys. Rev. B* **56**, 5049 (1997).
 - ³² M. K. Crawford, G. Burns, G. V. Chandrashekhar, F. H. Dacol, W. E. Farneth, E. M. McCarron, III, and R. J. Smalley, *Solid State Commun.* **73**, 507 (1990).
 - ³³ J. L. Peng, Z. Y. Li, and R. L. Greene, *Physica C* **177**, 79 (1991).
 - ³⁴ C. C. Homes, M. Reedyk, D. Crandles, and T. Timusk, *Appl. Opt.* **32**, 2972 (1993).
 - ³⁵ This finite conductivity effectively renders the sample opaque at room temperature and above. The origin of the fringes at low temperature is attributed to interference effects due to reflections from the back of the crystal as the sample becomes increasingly transparent, as evidenced by the unphysical results [$\sigma_1(\omega) < 0$] at low temperature.
 - ³⁶ Several overdamped Lorentzian oscillators have been included in the fits to reproduce the broad, incoherent absorption attributed to thermally-activated hopping. At room temperature the Drude component (a Lorentzian centered at zero frequency) is $\gamma_0 = 420$ and $\omega_{p,0} = 620$, the parameters for the two mid-infrared bands are: $\omega_1 = 1100$, $\gamma_1 = 1120$ and $\omega_{p,1} = 1270$; $\omega_2 = 4400$, $\gamma_2 = 1800$ and $\omega_{p,2} = 2200$. (All units are in cm^{-1}).
 - ³⁷ J. D. Perkins, R. J. Birgeneau, J. M. Graybeal, M. A. Kastner, and D. S. Kleinbert, *Phys. Rev. B* **58**, 9390 (1998).
 - ³⁸ A. S. Alexandrov and N. F. Mott, *Polarons and Bipolarons* (World Scientific, Singapore, 1995).
 - ³⁹ X.-X. Bi and P. C. Eklund, *Phys. Rev. Lett.* **70**, 2625 (1993).
 - ⁴⁰ T. Katsufuji, T. Tanabe, T. Ishikawa, Y. Fukuda, T. Arima, and Y. Tokura, *Phys. Rev. B* **54**, R14230 (1996).
 - ⁴¹ N. F. Mott and E. A. Davis, *Electronic Processes in Non-Crystalline Materials* (Clarendon, Oxford, 1971).
 - ⁴² V. Amgegaokar, B. I. Halperin, and J. S. Langer, *Phys. Rev. B* **4**, 2612 (1971).
 - ⁴³ Normal coordinate calculations, which are applicable to zero wavevector normal mode analysis, have an advantage over lattice dynamical calculations in that non-central forces such as those involved in angle bending may be treated. The effect of angle-bending force constants is proportional to the covalency of the compound (Ref. 55); given the estimated covalency of 0.5 for the cuprate systems (Ref. 56) they should be considered.
 - ⁴⁴ E. B. Wilson, Jr., J. C. Decius, and P. C. Cross, *Molecular Vibrations* (McGraw-Hill, New York, 1955).
 - ⁴⁵ T. Shimanouchi, M. Tsuboi, and T. Miyazawa, *J. Chem. Phys.* **35**, 1597 (1961).
 - ⁴⁶ E. Dowty, *VIBRATZ*, Shape Software.
 - ⁴⁷ J. L. Servoin, Y. Luspain, and F. Gervais, *Phys. Rev. B* **22**, 5501 (1980).
 - ⁴⁸ P. Dufour, S. Jandl, C. Thomsen, M. Cardona, B. M. Wanklyn, and C. Changkang, *Phys. Rev. B* **51**, 1053 (1995).
 - ⁴⁹ S. Jandl, M. Iliev, C. Thomsen, T. Ruf, and M. Cardona, *Solid State Commun.* **87**, 609 (1993).

- ⁵⁰ S. H. Wang, Q. Song, B. P. Clayman, J. L. Peng, L. Zhang, and R. N. Shelton, Phys. Rev. Lett. **64**, 1067 (1990).
- ⁵¹ S. Lupi, M. Capizzi, P. Calvani, R. Ruzicka, P. Maselli, P. Dore, and A. Paolone, Phys. Rev. B **57**, 1248 (1998).
- ⁵² X. K. Chen, J. C. Irwin, and J. P. Franck, Phys. Rev. B **52**, 13130 (1995).
- ⁵³ A. B. Kuz'menko, D. van der Marel, P. J. M. van Bentum, E. A. Tishchenko, C. Presura, and A. A. Bush, Phys. Rev. B **63**, 94303 (2001).
- ⁵⁴ C. C. Homes, B. P. Clayman, J. L. Peng, and R. L. Greene, Phys. Rev. B **56**, 5525 (1997).
- ⁵⁵ R. M. Martin, Phys. Rev. B **1**, 4005 (1970).
- ⁵⁶ L. Pauling, Phys. Rev. Lett. **59**, 225 (1988).